Journal of Alloys and Compounds 509 (2011) 9318–9321

Contents lists available at ScienceDirect

Journal of Alloys and Compounds

journal homepage: www.elsevier.com/locate/jallcom

Optical band gap tuning of discontinuous $[SnO_2/Mn]_n$ multilayers

S. Saipriya, R. Singh*

School of Physics, University of Hyderabad, Central University P.O., Hyderabad 500 046, India

ARTICLE INFO

Article history:
Received 4 April 2011
Received in revised form 7 July 2011
Accepted 8 July 2011
Available online 18 July 2011

Keywords:
Metal dielectric multilayers
Discontinuous multilayers
Surfaces and interfaces
Optical properties

ABSTRACT

Multilayers (ML) of $[SnO_2/Mn]_n$ were deposited by RF-magnetron sputtering on quartz substrates at room temperature using metal targets. The XRD pattern and the XRR show amorphous and discontinuous nature of ML respectively. The transmittance (at 550 nm) as well as the estimated optical band gap (E_g) decreases with the increase in the number of bilayers. The present study shows that the optical properties of the present ML can be tuned by changing the n value.

1. Introduction

Semiconductors have been used for centuries in electronics. Due to the presence of free carriers they are used extensively for applications which require high conductivity. Oxide semiconductors like ZnO, SnO_2, TiO_2, etc. possess high band gap (>3.2 eV) and are transparent in the visible region. Multilayers (ML) of these oxides with various metals give enhanced optical and magnetic properties than the corresponding doped systems [1]. They have various applications in GMR [2], solar cells [3], etc. They are easier to manipulate to achieve required optical properties and are useful in applications like plasmon lithography [4], UV band pass filters [5], gas sensors [6], photo catalyst [7], heat reflectors, eye protectors, etc.

Some of the factors which affect the band gap of ML are the number of layers [8], thickness of each layer [9,10] and lattice mismatch at the interface [11]. SnO_2 is a wide band gap (3.6 eV) semiconductor which is transparent in the visible region. ML of SnO_2 with Fe_2O_3 [6], TiO_2 [12] and CdO [13] has been used to enhance the gas sensing properties, as photocatalyst and to engineer the band gap respectively. These multilayers are often prone to pin holes which deteriorate their magnetic and transport properties.

A new class of materials called discontinuous ML has been gaining attention due to their enhanced magnetic and transport properties. In these materials the metallic particles are isolated by the insulator matrix, thereby minimizing the effect of pin holes. The magnetic nature of the metallic particles is well preserved by the surrounding matrix and results in high coercivity. Such discontinuous ML exhibit high resistivity, low field sensitivity [14] due to coulomb blockade, percolation and quantum size effects. Fabrication of these materials at room temperature is of great advantage. Alternate deposition of very thin layers of the metal and the insulator increases the concentration of defects like oxygen vacancies or interstitials at the interfaces [15]. The metal particles get embedded into the matrix when the thickness of the layers is comparable to the interface roughness. ML prepared by stacking layers of wide band gap semiconductor and metal alternately paves way in tuning the optical properties [16]. The enhanced optical properties in ML of metals and dielectrics is attributed to the phenomenon of surface plasmon resonances at the interface [17].

In the present work we report the fabrication of (SnO_2/Mn) discontinuous multilayers and their optical properties.

2. Experimental

ML of Mn and SnO_2 were deposited alternately on clean and unheated quartz substrates using RF magnetron sputtering system. The configuration of the system is described elsewhere [18]. The SnO_2 and Mn layers were deposited using high purity (99.99%) Sn and Mn target of 2 in. diameter. The deposition of SnO_2 layers was done in oxygen environment at partial pressure of 7.9 mTorr using 25 W of power. The deposition of Mn layers was done in argon environment at partial pressure of 4.5 mTorr using 45 W of power. The rate of deposition was determined by depositing SnO_2 and Mn layers individually. The thickness of each layer was controlled by controlling the duration of deposition. The structure of the ML is $[SnO_2\ x\text{ Å}/Mn\ y\text{ Å}]_n$ where n denotes the number of bilayers. In order to study the effect of bilayers, $[SnO_2$ 12 Å/Mn 24 Å$]_n$ with n = 5, 10, 20, 40 ad 60 bilayers were deposited.

The films were characterized using X-ray diffractometer (Inel XRG 3000) and XRR (Bruker) equipped with Co Kα radiation source. The total thickness of various ML was measured using a surface stylus profilometer (AMBIOS Tech Model XP-1). The reflectance and transmittance spectra in UV–vis–IR range were recorded at room temperature using a JASCO-670 spectrophotometer. The optical properties of the ML were compared with SnO_2 film of comparable thickness.

* Corresponding author. Tel.: +91 40 2313 4321; fax: +91 40 2301 0227.
E-mail address: rssp@uohyd.ernet.in (R. Singh).

0925-8388/$ – see front matter © 2011 Elsevier B.V. All rights reserved.
doi:10.1016/j.jallcom.2011.07.019

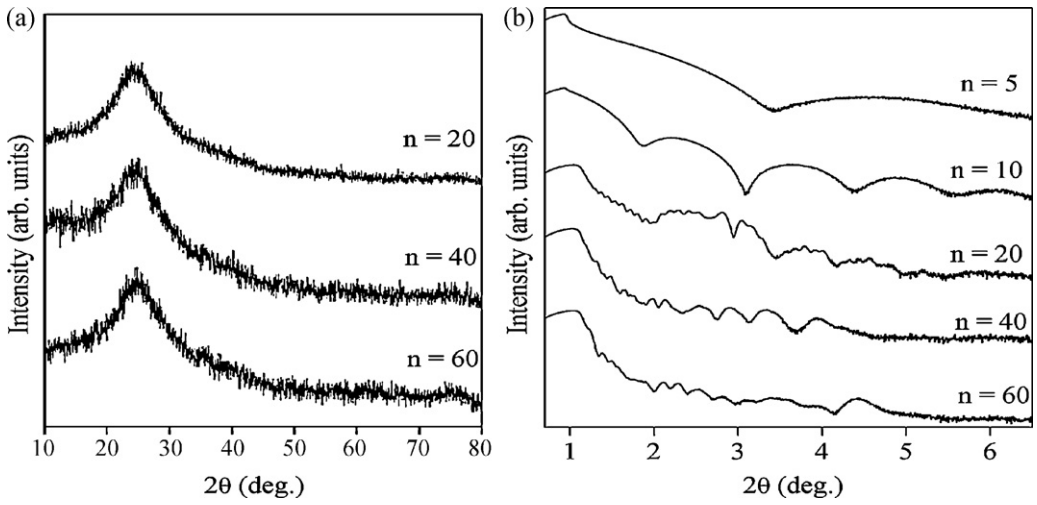

Fig. 1. (a) XRD pattern and (b) XRR spectra of $[SnO_2$ 12 Å/Mn 24 Å$]_n$ ML.

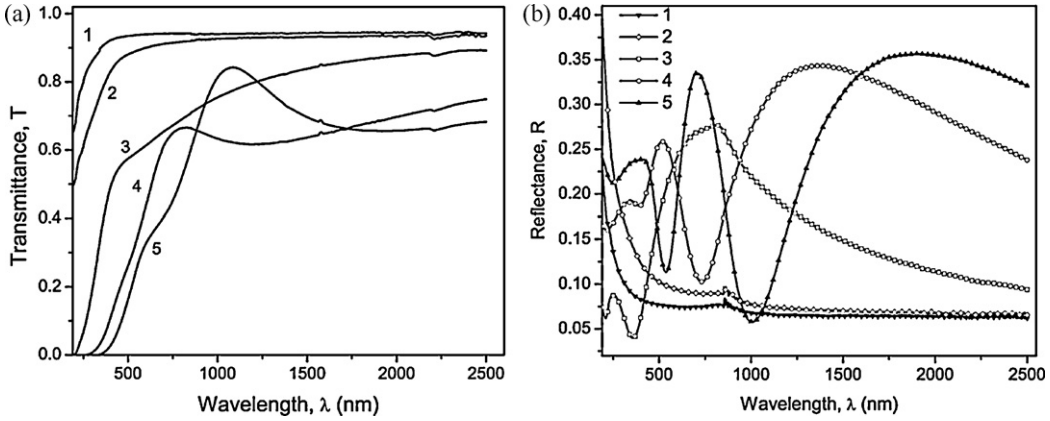

Fig. 2. (a) Transmittance and (b) reflectance spectra of $[SnO_2$ 12 Å/Mn 24 Å$]_n$ ML with (1) $n = 5$, (2) $n = 10$, (3) $n = 20$, (4) $n = 40$, and (5) $n = 60$.

3. Results and discussions

The normal XRD pattern for the ML shown in Fig. 1(a) indicates them to be amorphous. The X-ray reflectivity (XRR) studies shown in Fig. 1(b) provide the multilayer nature of all the samples. The presence of bilayer peaks in all the XRR spectra confirms that all the samples are multilayer structures [19]. The ML with $n = 5$ exhibits broad well separated fringes with very low amplitude. This is attributed to the lower thickness of the ML leading to diffuse scattering from the substrate [20]. The fringe width and separation between them decreases with increase in n. The non-periodic behavior of the fringes indicates the discontinuous nature of the ML [21,22].

The transmittance and reflectance at normal incidence for various ML are shown in Fig. 2. It can be clearly seen that the transmittance at 550 nm decreases and the reflectance increases with increasing number of bilayers. The fringes in the transmittance and reflectance spectra arise due to the interference of the light reflected by the substrate–film and film–air interfaces and internal reflections within the film. The maximum transmittance in the visible region for the ML is 75%. The transmittance increases and the reflectance decreases in the IR region for the ML. Fig. 2(a) also shows that the absorption edge shifts towards higher wavelength with increasing number of bilayers.

When an electromagnetic wave passes through a medium it gets attenuated due to free carrier absorption, scattering, generation of phonons, etc. The refractive index in such lossy medium is a complex quantity. The complex refractive index $\tilde{n}$, of a material is given by

$$\tilde{n} = n + ik \tag{1}$$

where the real part, n, represents normal refractive index of the material and the imaginary part, k, represents the extinction coefficient of the material. The n value is calculated from the reflectance data using the relation [23]

$$n = \frac{1 + \sqrt{R}}{1 - \sqrt{R}} \tag{2}$$

Fig. 3(a) shows the variation of n with the wavelength (λ). The refractive index exhibits an oscillatory behavior in the visible region between maximum and minimum values of 3.75 and 1.5 respectively. Then there is a continuous decrease up to 2 in the IR region.

The extinction coefficient represents the loss of the EM radiaion while travelling through the medium. It can be estimated using the relation

$$k = \frac{\alpha\lambda}{4\pi} \tag{3}$$

where the absorption coefficient (α) is a measure of the extent to which light is absorbed by the material as it passes through. α can be estimated using the relation

$$\alpha = -\frac{1}{t}(\ln(T)) \tag{4}$$

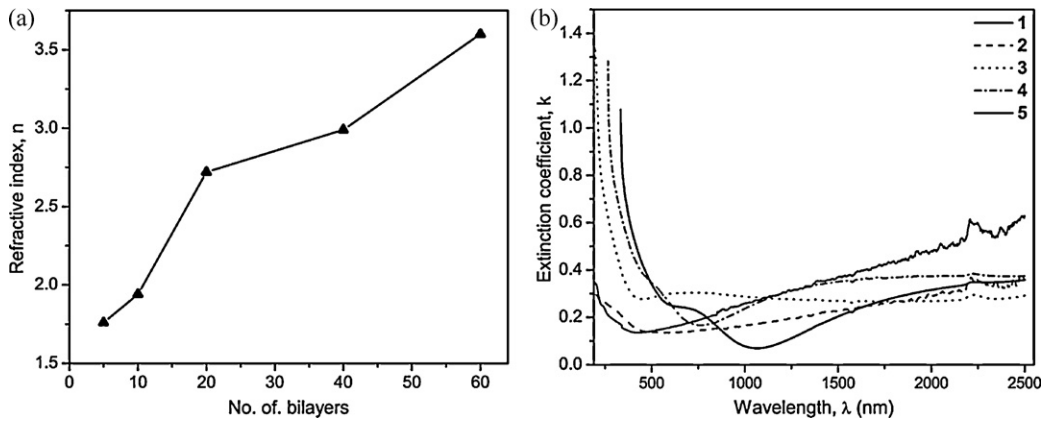

Fig. 3. (a) Refractive index, n and (b) extinction coefficient, k of $[SnO_2$ 12 Å/Mn 24 Å$]_n$ ML with (1) $n = 5$, (2) $n = 10$, (3) $n = 20$, (4) $n = 40$, and (5) $n = 60$.

Table 1
Thickness, RMS and optical parameters of SnO_2 film and $[SnO_2$ 12 Å/Mn 24 Å$]_n$ ML deposited in various process gas environment.

Sample id	Sample	Thickness (nm)	E_g (eV)	E_U (eV)	β ($\times 10^{-2}$)	n at 550 nm
1	SnO_2	225	4.56 ± 0.01	0.594 ± 0.009	5.38	2.8
2	$n = 5$	19	>6.5	–	–	–
3	$n = 10$	37	>6.5	–	–	–
4	$n = 20$	73	4.47 ± 0.03	1.562 ± 0.007	1.65	2.7
5	$n = 40$	153	2.84 ± 0.03	1.269 ± 0.013	2.04	3.0
6	$n = 60$	224	2.46 ± 0.03	0.772 ± 0.005	3.35	3.6

Fig. 3(b) shows the variation of k value with wavelength. It initially decreases with increase in wavelength, then remains constant. The extinction coefficient at 500 nm increases with increasing number of bilayers. The ML with 60 bilayers seem to have higher damping than the other ML. This might be due to increasing absorbance with increasing number of bilayers.

The optical band gap (E_g) of the films is calculated from the absorption coefficient using relation [24],

$$\alpha h\upsilon = A(h\upsilon - E_g)^m \tag{5}$$

where A is a constant, ($h\upsilon$) is the energy of incident photon and $m = 0.5$ and 2 for direct and indirect transitions respectively [23]. Fig. 4(a) shows $(\alpha h\upsilon)^2$ vs. $h\upsilon$ plot. The direct bandgap is obtained by extrapolating the linear part of the graph to $\alpha h\upsilon = 0$. The y-axis scale has been limited to 5% of transmittance since maximum absorption takes place in this region. The absorption edge for the ML with $n = 5$ and 10 occurs well below 190 nm which is beyond the limit of the instrument. Hence E_g values for these ML is greater than 6.5 eV. However, a rough estimation of E_g values for these ML is 12 and 10 eV for $n = 5$ and 10 respectively. Fig. 4(b) shows the variation of bandgap with the number of bilayers. E_g decreases with the increase in number of bilayers. The decrease of bandgap as n increases from $n = 40$ to $n = 60$ is less than for lower values of n.

Further, to measure the width of tail states, Urbach energy was calculated. The presence of tail states, initiates the absorption at energies lower than E_g. For energies lower than E_g there is an exponential decrease in absorption. In this region it neither obeys the Tauc's relation nor Mott and Davis's. Urbach proposed the following rule for absorption below E_g [25],

$$\alpha = \alpha_0 \exp\left[\frac{\beta}{k_B T}(h\upsilon - E)\right] \tag{6}$$

$$\alpha = \alpha_0 \exp\left[\frac{h\upsilon - E}{E_U}\right] \tag{7}$$

where β is the steepness factor and

$$\beta = \frac{k_B T}{E_U} \tag{8}$$

where E and α_0 are the constants characteristics of the material and E_U is the Urbach energy which refers to the width of the tail states. Urbach energy also determines the rate of decrease of α below the band gap. This exponential dependence of α is attributed to random fluctuations of the internal fields associated with the disorder in the material [26]. Urbach energy is sensitive to defects, strain and dangling bonds. Fig. 5 shows the plot of $\ln \alpha$ vs. $h\upsilon$. E_U is calculated from the slope of the plot using the relation

$$E_U = \left[\frac{d(\ln \alpha)}{d(h\upsilon)}\right]^{-1} \tag{9}$$

From Eq. (7) β is estimated. The values of E_g, E_U and β are listed in Table 1. The Urbach energy is found to decrease with increase in the number of bilayers. This might be due to decreasing disorder in the ML. ML with low thickness are found to be more strained. As the number of bilayer increases, the strain in the material decreases leading to low E_U values.

In order to study the effect of Mn incorporation, the optical properties of $[SnO_2$ 12 Å/Mn 24 Å$]_{60}$ ML is compared with that of SnO_2 film of same thickness deposited using Sn target reported elsewhere [27]. There is a significant decrease in transmittance and increase in refractive index of $[SnO_2$ 12 Å/Mn 24 Å$]_{60}$ when compared with SnO_2 thin film of same thickness presumably due to the Mn metallic content in the sample. The ML has lower E_g and higher E_U value compared with that of the SnO_2 film. The decrease in the E_g values may be attributed to the metallic nature of Mn whereas the increase in E_U values may be an interfacial effect. The mismatch at the interface induces defects in the ML which in turn may lead to increase in E_U value of the ML [28].

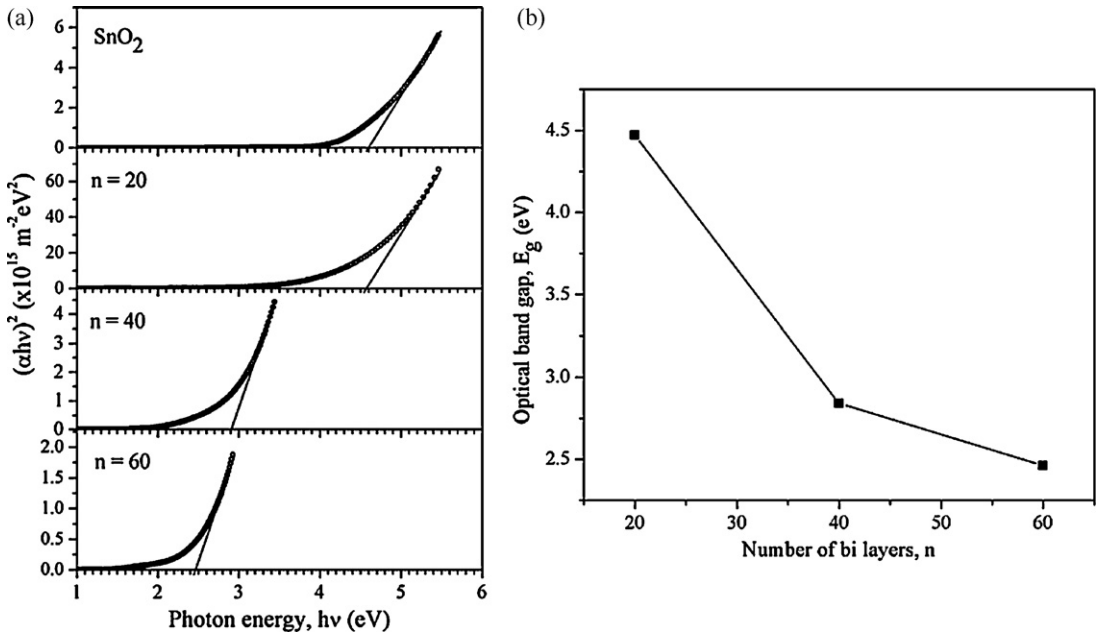

Fig. 4. (a) Plots of $(\alpha h\upsilon)^2$ vs. photon energy, $h\upsilon$ for (a) SnO_2 film and $[SnO_2$ 12 Å/Mn 24 Å$]_n$ ML. (b) Variation of band gap (E_g) with the number of bilayers.

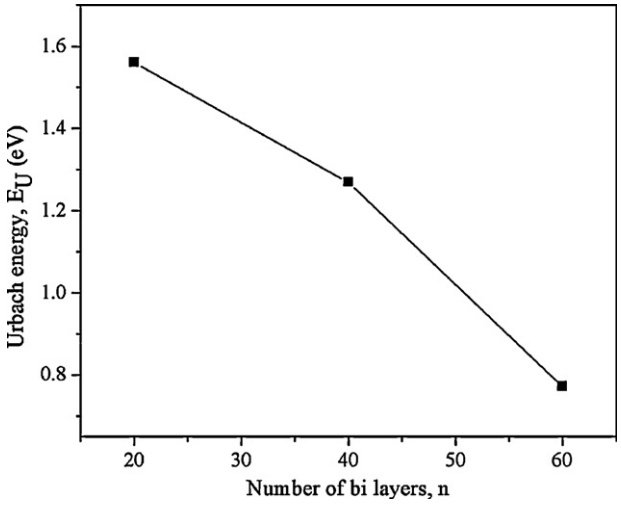

Fig. 5. Variation of Urbach energy of $[SnO_2$ 12 Å/Mn 24 Å$]_n$ ML with increasing number of bilayers.

4. Conclusions

SnO_2 thin film and $(SnO_2/Mn)_n$ ML were deposited using RF Magnetron sputtering. The films are amorphous in nature. The absence of periodicity in XRR spectra indicates the discontinuous nature of the ML. The optical properties of ML are strongly dependent on the number of bi-layers. The E_g value decreases on introduction of Mn layers, which can be attributed to metallic nature of Mn. The present work shows that by varying the number of bi-layers the optical band gap of metal-dielectric ML can be tuned.

Acknowledgement

S.S. acknowledges the financial support from CAS, School of Physics.

References

[1] L. Cattin, M. Morsli, F. Dahou, S. Yapi Abe, A. Khelil, J.C. Bernède, Thin Solid Films 518 (2010) 4560.
[2] M.N. Baibich, J.M. Broto, A. Fert, F. Nguyen Van Dau, F. Petroff, Phys. Rev. Lett. 61 (1988) 2472.
[3] P. Ravirajan, Adv. Funct. Mater. 15 (2005) 609.
[4] M. Joseph Roberts, A. Guenthner, G. Lindsay, S. Feng, Mater. Res. Soc. Symp. Proc. 919E (2006), 0919-J02-06.
[5] Z. Jakšić, M. Maksimović, M. Sarajlić, J. Opt. A: Pure Appl. Opt. 7 (2005) 51.
[6] Z. Jiao, S. Wang, L. Bian, J. Liu, Mater. Res. Bull. 35 (2000) 741.
[7] N. Kanai, Y. Fukunaga, M. Suzuki, T. Watanabe, K. Hashimoto, H. Ohsaki, Optical Interference Coatings, OSA Technical Digest Series (Optical Society of America, 2004), paper TuA5.
[8] M. Beaudoin, M. Meunier, C.J. Arsenault, Phys. Rev. B 47 (1993) 2197.
[9] D.R. Sahu, J.-L. Huang, Appl. Surf. Sci. 253 (2006) 915.
[10] A. Kaushal, D. Kaur, J. Alloys Compd. 509 (2011) 200–205.
[11] S. Tripathi, R. Brajpuriya, C. Mukharjee, S.M. Chaudhari, J. Mater. Res. 21 (2006) 623.
[12] H. Ohsaki, N. Kanai, Y. Fukunaga, M. Suzuki, T. Watanabe, K. Hashimoto, Thin Solid Films 502 (2006) 138.
[13] X. Li, Mater. Res. Soc. Symp. Proc. 804 (2004) JJ2.4.1.
[14] S. Sankar, B. Dieny, A.E. Berkowitz, J. Appl. Phys. 81 (1997) 5512.
[15] S.-S. Yan, C. Ren, X. Wang, Y. Xin, Z.X. Zhou, L.M. Mei, M.J. Ren, Y.X. Chen, Y.H. Liu, H. Garmestani, Appl. Phys. Lett. 84 (2004) 2376.
[16] Z. Wang, Vacuum 80 (2006) 438.
[17] H.-K. Park, J.-W. Kang, S.-I. Na, D.-Y. Kim, H.-K. Kim, Sol. Energy Mater. Sol. Cells 93 (2009) 1994.
[18] M. Sultan, R. Singh, J. Phys. D: Appl. Phys. 42 (2009) 115306.
[19] M. Jergel, et al., Superficies Vacio 8 (1999) 28.
[20] W.H. Briscoe, M. Chen, I.E. Dunlop, J. Klein, J. Penfold, R.M.J. Jacobs, J. Colloid Interface Sci. 306 (2007) 459.
[21] D.G. Kurth, V. Dirk, R. Michaela, B. Richter, A. Muller, Chem. Mater. 12 (2000) 2829.
[22] M. Löhmann, F. Klabunde, J. Bläsing, P. Veit, T. Drüsedau, Thin Solid Films 42 (3) (1999) 127.
[23] M. Fox, Optical Properties of Solids , Oxford University Press, New York, 2001.
[24] N.F. Mott, R.W. Gurney, Electronic Processes in Ionic Crystals , Dover Publications, New York, 1964.
[25] F. Urbarch, Phys. Rev. 92 (1953) 1324.
[26] Y. Caglar, S. Ilician, M. Caglar, Eur. Phys. J. B 58 (2007) 251.
[27] S. Saipriya, M. Sultan, R. Singh, Physica B 46 (2011) 812.
[28] R.B. Wehrspohna, J.-N. Chazalviel, F. Ozanam, I. Solomon, Eur. Phys. J. B 8 (1999) 179.